Electr Eng (2017) 99:1073–1085
DOI 10.1007/s00202-016-0467-1

ORIGINAL PAPER

Direct torque control of five-leg inverter-dual induction motor powertrain for electric vehicles

Bekheïra Tabbache[1] · Sofiene Douida[1] · Mohamed Benbouzid[2,4] · Demba Diallo[3] · Abdelaziz Kheloui[1]

Received: 3 February 2016 / Accepted: 31 October 2016 / Published online: 14 November 2016

Abstract This paper deals with the adaptation and implementation of an adaptive direct torque control for the five-leg inverter-dual induction machine drive. The expectations are to take advantage of the direct control benefits, which are: sensorless, ease of implementation, and robustness against parameters variation. The application focuses on an electric vehicle with two driving wheels. For this, both induction motors coupled to the driving wheel are fed through a five-leg power inverter. For that purpose, the structure of this vehicle requires an electric differential, which allows maintaining the stability of the vehicle and especially during cornering. For this, the proposed direct control can ensure the separate control and distribute the required torques to the induction motors. Experiments and simulations are carried out to show that the developed independent control of five-leg inverter is effective and provides a simple configuration with good performance in terms of speed and torque responses.

Keywords Electric vehicle · Electric differential · 5-Leg inverter · Induction motor · Direct torque control (DTC)

✉ Mohamed Benbouzid
Mohamed.Benbouzid@univ-brest.fr

Bekheïra Tabbache
laid_tabache@yahoo.com

Demba Diallo
demba.diallo@geeps.centralesupelec.fr

[1] Ecole Militaire Polytechnique, 16111 Algiers, Algeria

[2] University of Brest, FRE CNRS 3744 IRDL, Rue de Kergoat, CS 93837, 29238 Brest Cedex 03, France

[3] University of Paris Sud, UMR CNRS GEEPS, 11 Rue Joliot Curie, 91192 Gif-Sur-Yvette, France

[4] Shanghai Maritime University, 201306 Shanghai, China

Nomenclature

EV	Electric vehicle
IM	Induction motor
IFOC	Indirect field-oriented control
PWM	Pulse-width modulation
FG	Fixed gear
FLI	Five-leg inverter
ED	Electric differential
MD	Mechanic differential
s, (r)	Stator (rotor) index
α, β	Synchronous reference frame index
a, b, c	Three phases reference frame index
V (I)	Voltage (current)
R	Resistance
L (L_m)	Inductance (magnetizing inductance)
σ	Leakage coefficient, $\sigma = 1 - L_m^2/L_s L_r$
T_r	Rotor time constant ($T_r = L_r/R_r$)
T_s	Stator time constant ($T_s = L_s/R_s$)
p	pole-pair number
v	Vehicle speed
F_w	Road load
F_{ro}	Rolling resistance force
F_{sf}	Stokes or viscous friction force
F_{ad}	Aerodynamic drag force
F_{cr}	Climbing and downgrade resistance force
P_v	Vehicle driving power
J	Total inertia (rotor and load)
ω_m	Electric motor mechanical speed
T_B	Load torque accounting for friction and windage
T_L	Load torque
T_m	Electric motor torque
i	Transmission ratio
η_t	Transmission efficiency

ref	Reference index
δ	Steering angle

1 Introduction

Electrical technology development and economic issues lead to complex systems using multi-machines. Therefore, the conventional structures of these systems require more components, which lead to increasing the price and volume, such as: amount of silicon and additional cooling system for semiconductor power [1].

Moreover, a classical structure of multi-machine system needs a specific control for each electric machine and these additional components reduce the system reliability. Therefore, it is interesting to develop new structures to reduce the power electronic devices and design a more simple system. However, the drive must still be robust to power electronic device failures [2] and has the ability to operate in degraded mode [3].

In the literature, many structures of inverters have been treated and proposed for supplying two three-phase induction motors. One of these structures is composed of five legs (each leg has two power switches), in which only one leg is shared by both machines [1,4]. This structure can also be viewed as a degraded version of the classical structure (two three-leg inverters) in the case of one leg fault [5,6]. In terms of control, the common leg requires special control techniques to allow an independent operation of the two induction motors. For this, intensive research is constantly in progress using the field-oriented vector control (FOC). However, FOC technique suffers from parameter variation of the induction motor and in particular the rotor time constant. Moreover, it requires special pulse-width modulation strategies to ensure an efficient-separated modulation [7].

In this context, this paper deals with the adaptation and implementation of an adaptive direct torque control for the five-leg inverter-dual induction machine drive. The expectations are to take advantage of the direct control benefits, which are: sensorless, ease of implementation, and robustness against parameters variation. The proposed traction system for electric vehicle in this paper optimizes the EV configuration with effective control in terms of cost and robustness.

The paper is organized as follows:

The first section deals with the structure and modeling of the five-leg inverter-dual induction motor drive with isolated neutral points. It also presents the principle of independent control. The second section introduces the proposed direct torque control of the five-leg inverter. For this, three switching tables are given to ensure the independent control of both induction motors. The third section is dedicated to the simulation results with different reference speeds and load torques. In Sect. 4, the paper presents the adaptation of the proposed system to the electric vehicle powertrain. Indeed, five-leg inverter-dual induction motor powertrain is used to propel two wheels. In this context, a decoupled control is developed taking into account electric vehicle dynamic. The developed control is also used to ensure vehicle stability with the electric differential during cornering. In Sect. 5, experimental results of the decoupled control are presented and discussed. Finally, a summary of the main ideas and performances is presented and a conclusion closes the paper.

2 five-Leg inverter-dual induction motor structure

In classical configuration, each induction motor is connected to a three-phase voltage PWM inverter. All systems are composed of six power legs in which each inverter contains three legs (each leg has two power switches). In Fig. 1, inverter legs A_1, B_1, and C_1 are connected to M_1, where as inverter legs A_2, B_2, and C_2 are connected to M_2.

Figure 2 shows the five-leg inverter (FLI) associated with two induction motors. In the FLI topology, both motors share one power leg (denoted leg C in this case). The other legs are connected to the motors as follows: A_1, B_1– a_1, and b_1 (a and b phases of motor 1), respectively, and A_2, B_2–a_2, and b_2 (a and b phases of motor 1), respectively [8,9].

Comparing the two topologies, one can notice a reduction of the number of power switches (10 against 12) with an expected reduction of volume and losses.

In the following, N1 and N2 are the motors M1 and M2 neutral points, respectively.

The Boolean control variables are denoted S_{ij} with $i = 1, 2, 3, 4, 5$ and $j = 1, 2$, and the power switches are assumed ideal.

From Fig. 2, the following equations can be derived:

$$\begin{cases} V_{\mathrm{A1N1}} = V_{\mathrm{A1O}} + V_{\mathrm{ON1}} \\ V_{\mathrm{B1N1}} = V_{\mathrm{B1O}} + V_{\mathrm{ON1}} \\ V_{\mathrm{CN1}} = V_{\mathrm{CO}} + V_{\mathrm{ON1}} \\ V_{\mathrm{A2N2}} = V_{\mathrm{A2O}} + V_{\mathrm{ON2}} \\ V_{\mathrm{B2N2}} = V_{\mathrm{B2O}} + V_{\mathrm{ON2}} \\ V_{\mathrm{CN2}} = V_{\mathrm{CO}} + V_{\mathrm{ON2}} \end{cases} \tag{1}$$

Under the assumption that the loads are balanced, it follows

$$\begin{cases} V_{\mathrm{A1N1}} + V_{\mathrm{B1N1}} + V_{\mathrm{CN1}} = 0 \\ V_{\mathrm{A2N2}} + V_{\mathrm{B2N2}} + V_{\mathrm{CN2}} = 0 \end{cases} \tag{2}$$

Therefore

$$\begin{cases} V_{\mathrm{ON1}} = -\frac{1}{3}\left(V_{\mathrm{A1O}} + V_{\mathrm{B1O}} + V_{\mathrm{CO}}\right) \\ V_{\mathrm{ON2}} = -\frac{1}{3}\left(V_{\mathrm{A2O}} + V_{\mathrm{B2O}} + V_{\mathrm{CO}}\right) \end{cases} \tag{3}$$

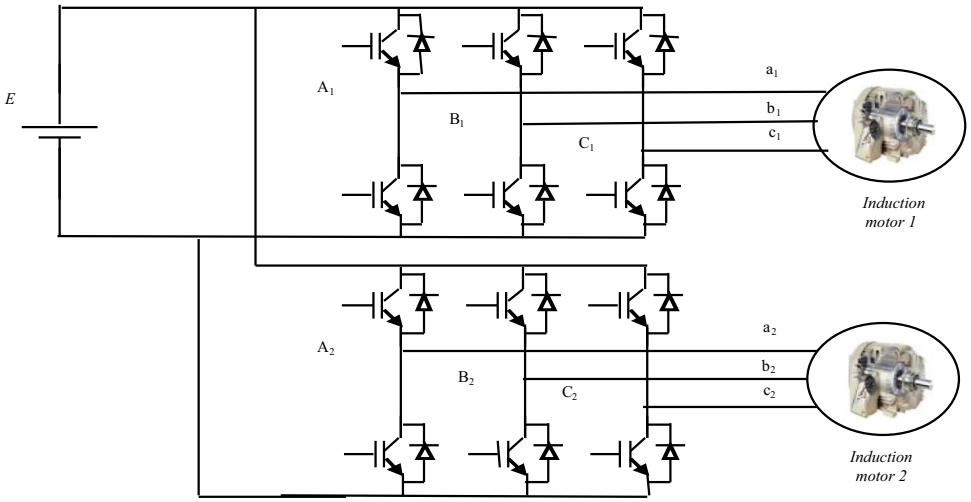

Fig. 1 Classical configuration

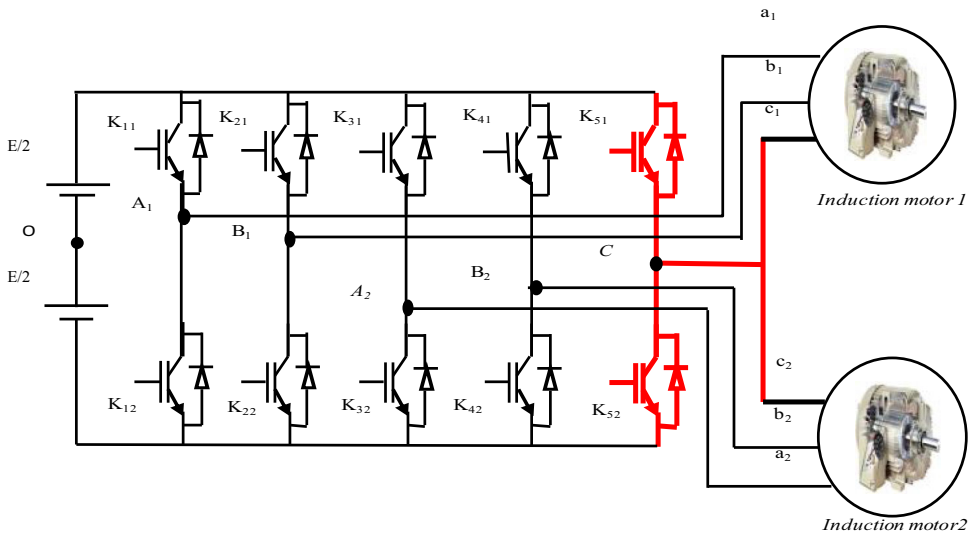

Fig. 2 Five-leg inverter-dual induction motor structure

The substitution of (3) in (1) leads to

$$\begin{cases} V_{\mathrm{A1N1}} = \frac{2}{3}V_{\mathrm{A1O}} - \frac{1}{3}V_{\mathrm{B1O}} - \frac{1}{3}V_{\mathrm{CO}} \\ V_{\mathrm{B1N1}} = -\frac{1}{3}V_{\mathrm{A1O}} + \frac{2}{3}V_{\mathrm{B1O}} - \frac{1}{3}V_{\mathrm{CO}} \\ V_{\mathrm{CN1}} = -\frac{1}{3}V_{\mathrm{A1O}} - \frac{1}{3}V_{\mathrm{B1O}} + \frac{2}{3}V_{\mathrm{CO}} \\ V_{\mathrm{A2N2}} = \frac{2}{3}V_{\mathrm{A2O}} - \frac{1}{3}V_{\mathrm{B2O}} - \frac{1}{3}V_{\mathrm{CO}} \\ V_{\mathrm{B2N2}} = -\frac{1}{3}V_{\mathrm{A2O}} + \frac{2}{3}V_{\mathrm{B2O}} - \frac{1}{3}V_{\mathrm{CO}} \\ V_{\mathrm{CN2}} = -\frac{1}{3}V_{\mathrm{A2O}} - \frac{1}{3}V_{\mathrm{B2O}} + \frac{2}{3}V_{\mathrm{CO}} \end{cases} \tag{4}$$

Considering the control variables, the inverter output voltages can be written as

$$\begin{cases} V_{\mathrm{A1O}} = (2S_{11} - 1)\frac{E}{2} \\ V_{\mathrm{B1O}} = (2S_{21} - 1)\frac{E}{2} \\ V_{\mathrm{A2O}} = (2S_{31} - 1)\frac{E}{2} \\ V_{\mathrm{B2O}} = (2S_{41} - 1)\frac{E}{2} \\ V_{\mathrm{CO}} = (2S_{51} - 1)\frac{E}{2} \end{cases} \tag{5}$$

Substituting (5) in (4) gives

$$\begin{bmatrix} V_{\mathrm{A1N1}} \\ V_{\mathrm{B1N1}} \\ V_{\mathrm{CN1}} \\ V_{\mathrm{A2N2}} \\ V_{\mathrm{B2N2}} \\ V_{\mathrm{CN2}} \end{bmatrix} = \frac{E}{3}\begin{bmatrix} 2 & -1 & 0 & 0 & -1 \\ -1 & 2 & 0 & 0 & -1 \\ -1 & -1 & 0 & 0 & 2 \\ 0 & 0 & 2 & -1 & -1 \\ 0 & 0 & -1 & 2 & -1 \\ 0 & 0 & -1 & -1 & 2 \end{bmatrix}\begin{bmatrix} S_{11} \\ S_{21} \\ S_{31} \\ S_{41} \\ S_{51} \\ . \end{bmatrix} \tag{6}$$

3 Direct torque control of five-leg inverter-dual induction motors

The control scheme of the induction motors associated with the five-leg inverter is presented in Fig. 3. The implementation control should ensure the separate control of both induction motors in terms of flux, torque, and speed.

In this paper, the independent control is based on direct torque control and an adapted switching table. The stan-

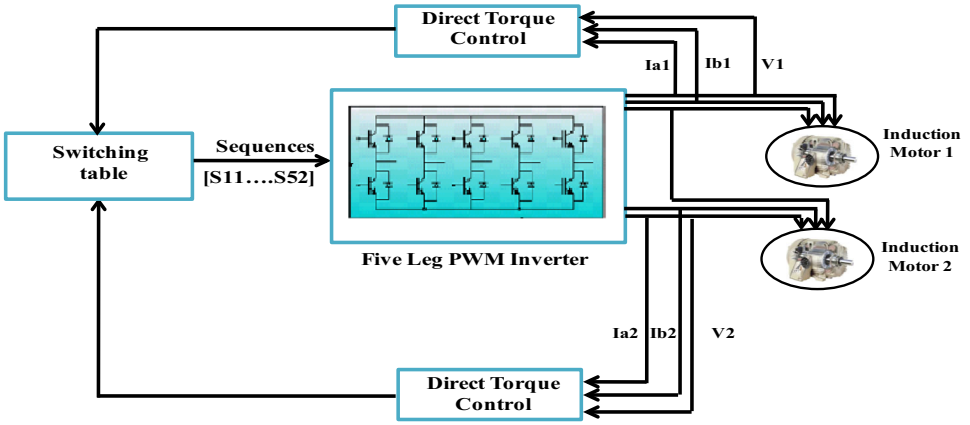

Fig. 3 Independent control scheme

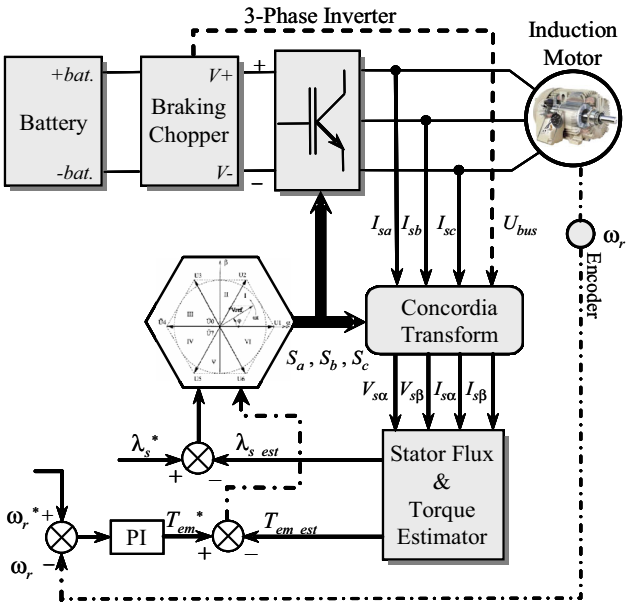

Fig. 4 DTC speed control block diagram

dard DTC does not require a mechanical sensor. However, in the case of electrical vehicle, a speed sensor is included in the drive. Therefore, in our case, a speed control loop with a proportional integral (PI) controller is designed to improve the dynamic performances; its output is the torque reference. Figure 4 displays this structure for one induction motor.

The flux and torque controls are carried out with hysteresis comparators and a switching logic table to selecting the appropriate inverter voltage [10].

Stator flux is estimated through the input voltage and the ohmic voltage drop:

$$\bar{\psi} = \int_0^t \left(\overline{v_s} - r_s \overline{i_s}\right) \mathrm{d}t. \tag{7}$$

Stator flux components in the (α, β) frame are given by

$$\begin{cases} \psi_{s\alpha} = \int_0^t \left(v_{s\alpha} - r_s i_{s\alpha}\right) \mathrm{d}t \\ \psi_{s\beta} = \int_0^t \left(v_{s\beta} - r_s i_{s\beta}\right) \mathrm{d}t \end{cases} \tag{8}$$

Motor torque is estimated using the following expression:

$$\Gamma = p\left(\psi_{s\alpha} i_{s\beta} - \psi_{s\beta} i_{s\alpha}\right) \tag{9}$$

4 The proposed switching table for the direct torque control of five-leg inverter

The DTC basic idea is to calculate flux and torque instantaneous values only from the stator variables. The control is carried out by hysteresis comparators of the flux and torque ($S_{\varphi s}$ and S_{ce}, respectively), the position of the stator flux vector in the (α, β) reference frame (denoted as the sector number $N_{i(i=1\ldots6)}$), and switching logic table selecting the appropriate voltage inverter configurations [11–13].

4.1 Vector representation of the three-phase power inverter

The output vector of a three-phase inverter (Fig. 5) can be represented by three Boolean control variables $S_j\,(j = a, b, c)$):

- $S_j = 1$: upper switch closed, lower switch opened.
- $S_j = 0$: upper switch opened, lower switch closed.

Eight output vectors can be obtained by the combinations of (S_a, S_b, S_c) with two null vectors: $(S_a, S_b, S_c) = (1, 1, 1)$ and $(S_a, S_b, S_c) = (0, 0, 0)$. Table 1 presents a switching table for the direct torque control [14]. The selection of zero vectors is based on different rules, such, for example, as the reduction the power switches losses.

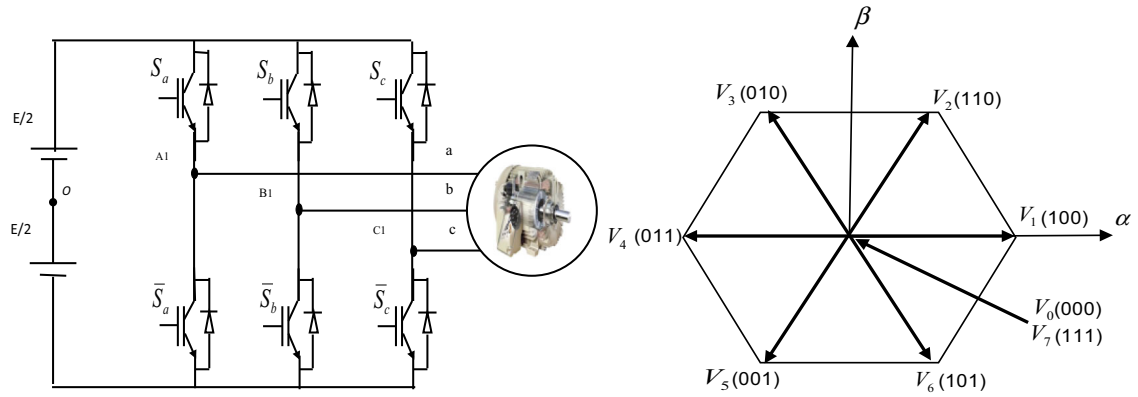

Fig. 5 Three-phase power inverter and its vectors representation

Table 1 Switching table with zero voltage vectors

Flux	Torque	Sector					
		1	2	3	4	5	6
$S_{\varphi s}=1$	$S_{ce}=1$	$V_2(1,1,0)$	$V_3(0,1,0)$	$V_4(0,1,1)$	$V_5(0,0,1)$	$V_6(1,0,1)$	$V_1(1,0,0)$
	$S_{ce}=0$	$V_7(1,1,1)$	$V_0(0,0,0)$	$V_7(1,1,1)$	$V_0(0,0,0)$	$V_7(1,1,1)$	$V_0(0,0,0)$
$S_{\varphi s}=0$	$S_{ce}=1$	$V_3(0,1,0)$	$V_4(0,1,1)$	$V_5(0,0,1)$	$V_6(1,0,1)$	$V_1(1,0,0)$	$V_2(1,1,0)$
	$S_{ce}=0$	$V_0(0,0,0)$	$V_7(1,1,1)$	$V_0(0,0,0)$	$V_7(1,1,1)$	$V_0(0,0,0)$	$V_7(1,1,1)$

Table 2 Switching table with permutation between null vectors

Flux	Torque	Sector					
		1	2	3	4	5	6
$S_{\varphi s}=1$	$S_{ce}=1$	V_2	V_3	V_4	V_5	V_6	V_1
	$S_{ce}=0$	V_7/V_0	V_7/V_0	V_7/V_0	V_7/V_0	V_7/V_0	V_7/V_0
$S_{\varphi s}=0$	$S_{ce}=1$	V_3	V_4	V_5	V_6	V_1	V_2
	$S_{ce}=0$	V_7/V_0	V_7/V_0	V_7/V_0	V_7/V_0	V_7/V_0	V_7/V_0

4.2 Switching table for five-leg inverter-dual induction motor

The effect of a zero vector is the same whatever the position of the stator flux. Therefore, the location of the zero voltage vectors can be permuted, as displayed in Table 2.

Table 2 is used to develop the switching table of DTC for the two induction motors feeding by a five-leg inverter.

If we denote V_{s1} (S_{a1}, S_{b1}, S_{c1}) and V_{s2} (S_{a2}, S_{b2}, S_{c2}), respectively, the voltage applied to the first and second motors according to variables $\left(S_{\psi_{si}}, S_{c_{ei}}, S_i\right)$ $(i = 1, 2)$, they are set according to the following rules:

If $(S_{ce1}, S_{ce2}) = (0, 1)$, the vector to be applied is $V_s\,(S_{c2}, S_{c2}, S_{a2}, S_{b2}, S_{c2})$.
If $(S_{ce1}, S_{ce2}) \neq (0, 1)$, the vector to be applied is

$$V_s\,(S_{a1}, S_{b1}, S_{a2}, S_{b2}, S_c) \quad \text{if } (S_{c1} = S_{c2} = S_c)\,.$$

$$V_s\,(S_{a1}, S_{b1}, S_{c1}, S_{c1}, S_{c1}) \quad \text{if } (S_{c1} \neq S_{c2})\,.$$

To summarize, the switching tables of the five-leg inverter are synthesized with the following rules:

- If $S_{ce1} = 1$ and $S_{ce2} = 1$, Table 3 is applied.
- If $S_{ce1} = 1$ and $S_{ce2} = 0$, Table 4 is applied.
- If $S_{ce1} = 0$ and $S_{ce2} = 1$, Table 5 is applied.
- If $S_{ce1} = 0$ and $S_{ce2} = 0$, the same zero vector is applied to both motors.

4.3 Alternative application of the sequences control

Based on the above logic, the switching table for DTC of five-leg inverter can be developed. However, in this case, one of the machines is not driven in an optimal way. Therefore, to mitigate these drawbacks, the applied sequence is selected alternatively (at half the sampling period) between the two tables.

The overall structure of this method is displayed in Fig. 6.

4.4 Simulation results

To illustrate the performance of the proposed control, simulations are carried out which two induction motors are used (Appendix). For this, different load torques and reference speeds are given to perform the independent control. The reference flux is set to 0.7 Web for the both induction motor.

Table 3 Switching table $S_{ce1} = 1$ and $S_{ce2} = 1$

$S_{ce2}=1$ \ $S_{ce1}=1$		Sector 1		Sector2		Sector 3		Sector 4		Sector 5		Sector 6	
		$S_{\varphi s1}=1$	$S_{\varphi s1}=0$	$S_{\varphi s1}=1$	$S_{\varphi s1}=0$	$S_{\varphi s1}=1$	$S_{\varphi s1}=0$	$S_{\varphi s1}=1$	$S_{\varphi s1}=0$	$S_{\varphi s1}=1$	$S_{\varphi s1}=0$	$S_{\varphi s1}=1$	$S_{\varphi s1}=0$
Sector1	$S_{\varphi s2}=1$	V_2 / V_2	V_3 / V_2	V_3 / V_2	V_4 / V_7	V_4 / V_7	V_5 / V_7	V_5 / V_7	V_6 / V_7	V_6 / V_7	V_1 / V_2	V_1 / V_2	V_2 / V_2
	$S_{\varphi s2}=0$	V_2 / V_3	V_3 / V_3	V_3 / V_3	V_4 / V_7	V_4 / V_7	V_5 / V_7	V_5 / V_7	V_6 / V_7	V_6 / V_7	V_1 / V_3	V_1 / V_3	V_2 / V_3
Sator2	$S_{\varphi s2}=1$	V_2 / V_3	V_3 / V_3	V_3 / V_3	V_4 / V_7	V_4 / V_7	V_5 / V_7	V_5 / V_7	V_6 / V_7	V_6 / V_7	V_1 / V_3	V_1 / V_3	V_2 / V_3
	$S_{\varphi s2}=0$	V_2 / V_0	V_3 / V_0	V_3 / V_0	V_4 / V_4	V_4 / V_4	V_5 / V_4	V_5 / V_4	V_6 / V_4	V_6 / V_4	V_1 / V_0	V_1 / V_0	V_2 / V_0
Sator3	$S_{\varphi s2}=1$	V_2 / V_0	V_3 / V_0	V_3 / V_0	V_4 / V_4	V_4 / V_4	V_5 / V_4	V_5 / V_4	V_6 / V_4	V_6 / V_4	V_1 / V_0	V_1 / V_0	V_2 / V_0
	$S_{\varphi s2}=0$	V_2 / V_0	V_3 / V_0	V_3 / V_0	V_4 / V_5	V_4 / V_5	V_5 / V_5	V_5 / V_5	V_6 / V_5	V_6 / V_5	V_1 / V_0	V_1 / V_0	V_2 / V_0
Sator4	$S_{\varphi s2}=1$	V_2 / V_0	V_3 / V_0	V_3 / V_0	V_4 / V_5	V_4 / V_5	V_5 / V_5	V_5 / V_5	V_6 / V_5	V_6 / V_5	V_1 / V_0	V_1 / V_0	V_2 / V_0
	$S_{\varphi s2}=0$	V_2 / V_0	V_3 / V_0	V_3 / V_0	V_4 / V_6	V_4 / V_6	V_5 / V_6	V_5 / V_6	V_6 / V_6	V_6 / V_6	V_1 / V_0	V_1 / V_0	V_2 / V_0
Sator5	$S_{\varphi s2}=1$	V_2 / V_0	V_3 / V_0	V_3 / V_0	V_4 / V_6	V_4 / V_6	V_5 / V_6	V_5 / V_6	V_6 / V_6	V_6 / V_6	V_1 / V_0	V_1 / V_0	V_2 / V_0
	$S_{\varphi s2}=0$	V_2 / V_1	V_3 / V_1	V_3 / V_1	V_4 / V_7	V_4 / V_7	V_5 / V_7	V_5 / V_7	V_6 / V_7	V_6 / V_7	V_1 / V_1	V_1 / V_1	V_2 / V_1
Sator6	$S_{\varphi s2}=1$	V_2 / V_1	V_3 / V_1	V_3 / V_1	V_4 / V_7	V_4 / V_7	V_5 / V_7	V_5 / V_7	V_6 / V_7	V_6 / V_7	V_1 / V_1	V_1 / V_1	V_2 / V_1
	$S_{\varphi s2}=0$	V_2 / V_2	V_3 / V_2	V_3 / V_2	V_4 / V_7	V_4 / V_7	V_5 / V_7	V_5 / V_7	V_6 / V_7	V_6 / V_7	V_1 / V_2	V_1 / V_2	V_2 / V_2

Table 4 Switching table if $S_{ce1} = 1$ and $S_{ce2} = 0$

$S_{ce2}=0$ \ $S_{ce1}=1$	Sector 1		Sector2		Sector 3		Sector 4		Sector 5		Sector 6	
	$S_{\varphi s1}=1$	$S_{\varphi s1}=0$	$S_{\varphi s1}=1$	$S_{\varphi s1}=0$	$S_{\varphi s1}=1$	$S_{\varphi s1}=0$	$S_{\varphi s1}=1$	$S_{\varphi s1}=0$	$S_{\varphi s1}=1$	$S_{\varphi s1}=0$	$S_{\varphi s1}=1$	$S_{\varphi s1}=0$
For any $S_{\varphi s2}$, N_2	V_2 / V_0	V_3 / V_0	V_3 / V_0	V_4 / V_7	V_4 / V_7	V_5 / V_7	V_5 / V_7	V_6 / V_7	V_6 / V_7	V_1 / V_0	V_1 / V_0	V_2 / V_0

Table 5 Switching table if $S_{ce1} = 0$ and $S_{ce2} = 1$

$S_{ce1}=0$ \ $S_{ce2}=1$	Sector 1		Sector2		Sector 3		Sector 4		Sector 5		Sector 6	
	$S_{\varphi s2}=1$	$S_{\varphi s2}=0$	$S_{\varphi s2}=1$	$S_{\varphi s2}=0$	$S_{\varphi s2}=1$	$S_{\varphi s2}=0$	$S_{\varphi s2}=1$	$S_{\varphi s2}=0$	$S_{\varphi s2}=1$	$S_{\varphi s2}=0$	$S_{\varphi s2}=1$	$S_{\varphi s2}=0$
For any $S_{\varphi s1}$, N_1	V_2 / V_0	V_3 / V_0	V_3 / V_0	V_4 / V_7	V_4 / V_7	V_5 / V_7	V_5 / V_7	V_6 / V_7	V_6 / V_7	V_1 / V_0	V_1 / V_0	V_2 / V_0

In Fig. 7, three reference torques are given for the first motor: 3, 2, and 1 N m and two references torques to the second motor for the first machine: 2 and 2.5 Nm. Figure 7 shows the responses of the proposed control in terms of induction motor torques. The torque response of the first and second motors is given, respectively, by the green and blue lines. This figure illustrates the performance of the independent control.

Figure 8a, b shows the stator currents of the both induction motors. These figures illustrate that both induction motors absorb sinusoidal currents.

Figure 9a, b shows the two components of the flux ($\varphi_{\alpha s1}$, $\varphi_{\beta s1}$) and ($\varphi_{\alpha s2}$, $\varphi_{\beta s2}$). These components design circular trajectory of each induction motors.

Figure 10 illustrates the induction motor response in terms of speeds. The first and second induction motor speeds are given, respectively, by the green and blue lines. It shows the performances of the independent control, in which the reference speeds are tracked perfectly.

Figure 11 gives the current in the common leg of the five-leg inverter.

Figure 11a shows the current in the case of the same reference speeds. In this case, the common leg provides sinusoidal

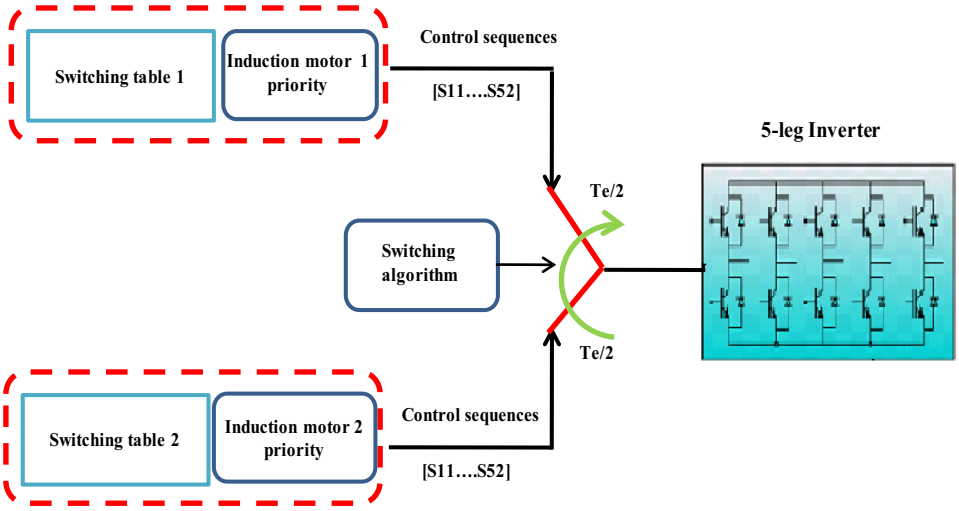

Fig. 6 Alternative application of the switching tables

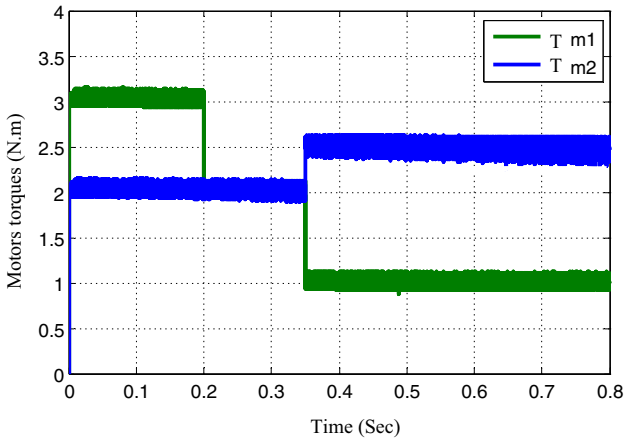

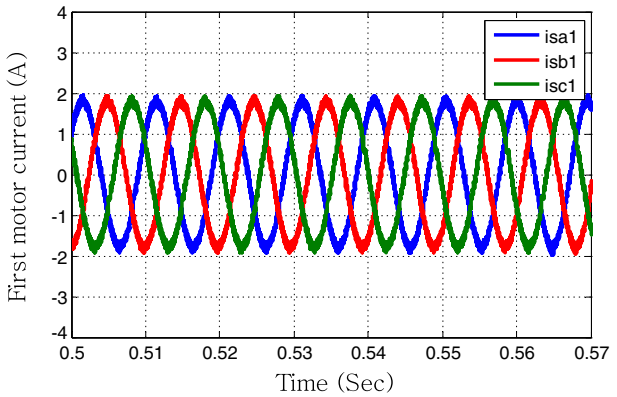

(a) Current of the first induction motor.

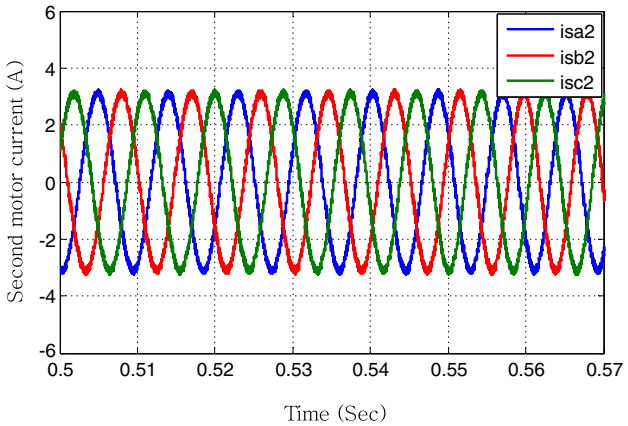

(b) Current of the second induction motor.

Fig. 7 Induction motor torques

Fig. 8 Induction motor currents

current, in which amplitude equals two times of each induction motor current, and the frequency is the same.

Figure 11b illustrates the shared less current in different reference speeds. It contains both frequencies of the induction motor currents.

It can be concluded that the proposed independent control based on direct torque control gives a promising performance in terms of speed and flux.

5 Five-leg inverter-dual induction motor EV powertrain

There are several possible EV configurations regarding the electric propulsion and the energy sources [15]. In

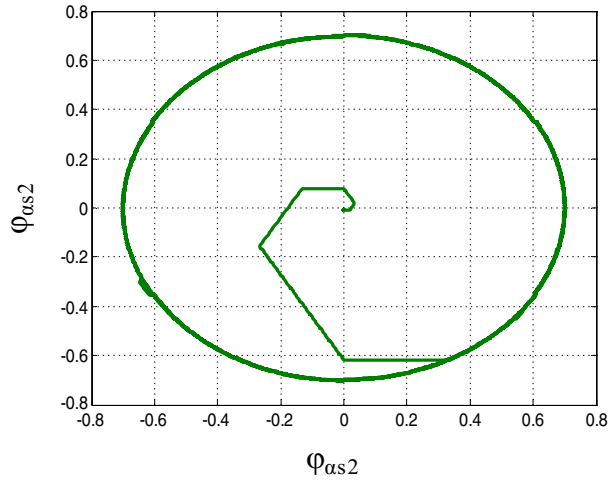

(a) Second induction motor flux components.

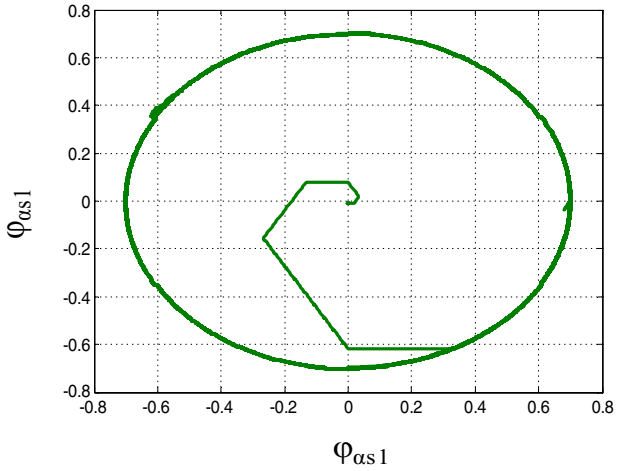

(b) First induction motor flux components.

Fig. 9 Induction motor stator flux

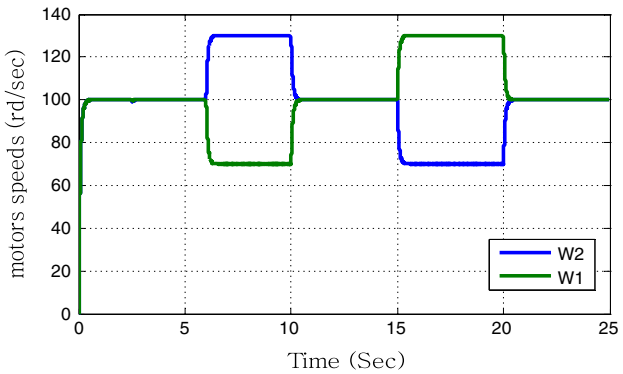

Fig. 10 Induction motor speeds

the adopted dual-motor configuration, two three-phase inverters are associated with two induction motors in front of the electric vehicle, as displayed in Fig. 12. In this work, both

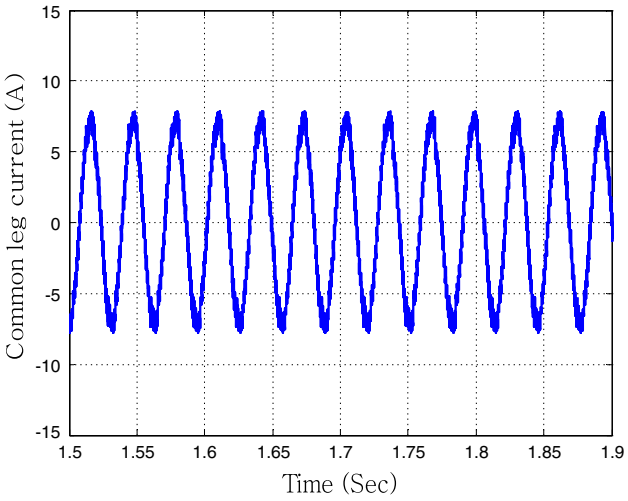

(a) Current with same reference speeds.

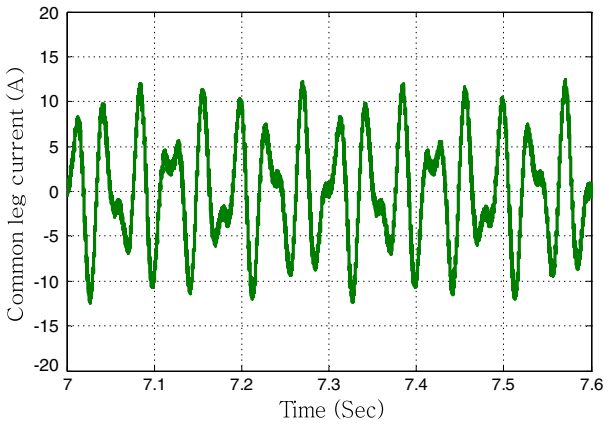

(b) Current with different reference speeds.

Fig. 11 Common leg current

induction motors are fed through a five-leg power inverter (Fig. 13).

5.1 Electric vehicle modeling and dynamics briefly

The proposed strategy takes into account the EV aerodynamics, and is not applied to the sole induction motor. The vehicle model is based on mechanics and aerodynamics principles [16].

The road load is then given by

$$F_w = F_{\text{ro}} + F_{\text{sf}} + F_{\text{ad}} + F_{\text{cr}}. \tag{10}$$

The power required to drive the EV at a speed v has to compensate the road load F_w:

$$P_v = vF_w. \tag{11}$$

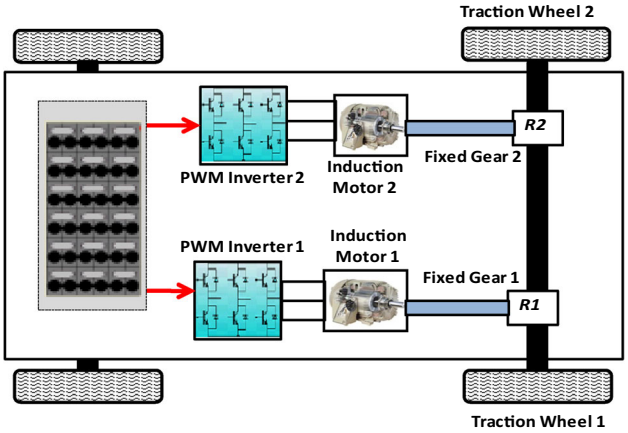

Fig. 12 EV dual induction motors fed by six-leg PWM inverter

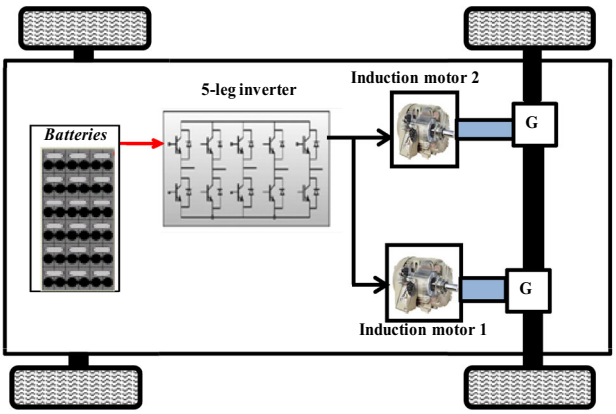

Fig. 13 EV dual induction motors fed by five-leg inverter

The mechanical equation (in the motor referential) used to describe each wheel drive is expressed by

$$J\frac{\mathrm{d}\omega_m}{\mathrm{d}t} + T_B + T_L = T_m. \tag{12}$$

The following equation is derived due to the use of a reduction gear:

$$\begin{cases} \omega_{\text{Wheel}} = \frac{\omega_m}{i} \\ T_{\text{Wheel}} = T_m i \eta_t \end{cases} \tag{13}$$

5.2 Electric differential

In two-wheel EV configuration, both induction motors are directly coupled with wheels to simplify the mechanical structure and, therefore, reduce the cost and the weight of vehicle powertrain. For that purpose, the structure of this vehicle requires an electric differential, which allows maintaining the stability of the vehicle and especially during cornering. The main task of the electric differential is to distribute the required torques to the induction motors [17].

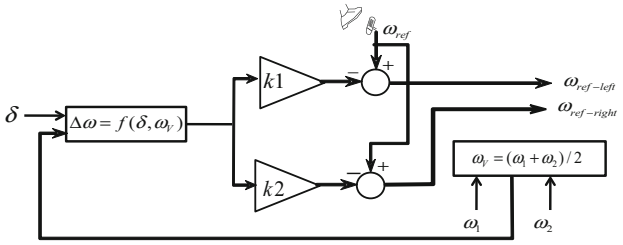

Fig. 14 Electric differential scheme

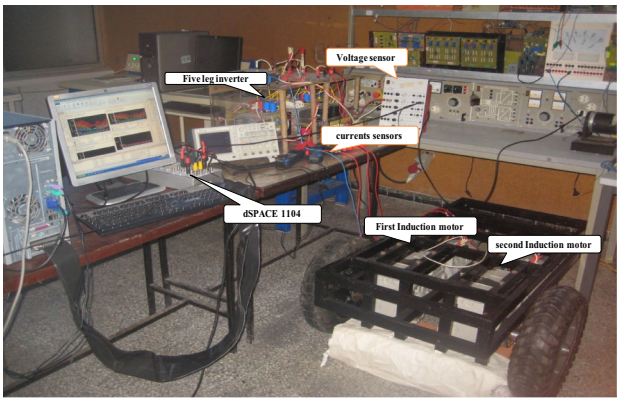

Fig. 15 Experimental test bench

The principle of the electric differential is shown in Fig. 14 [18]. For the straight-line regime, the motor rotation speeds have the same value. For cornering, the rotation speeds for each motor must be different [19,20].

6 Experimental results

6.1 Test bench

The test bench used to validate the proposed control strategies is illustrated in Fig. 15. The main components, in addition to the two 6kW induction motor fixed gears, are: (1) a dSPACE1104 development board interfaced to a standard PC; (2) Hall-effect sensors for voltage and current measurements (Ammeter pincers); (3) a five-leg power-inverter-based IGBT; and (4) two fixed gears.

The measured voltage and current provide voltages adapted to the input of dSPACE1104.

Experimental results are carried out to evaluate the proposed DTC for the five-leg inverter-dual induction motor powertrain. The rated parameters of the induction motors are given in the appendix.

In this section, the independent control is tested only by the reference torques given to each of the motors.

It should be noticed that experimental results are measured by serial communication RS232 connected to a TeKtronicx TDS2024 oscilloscope.

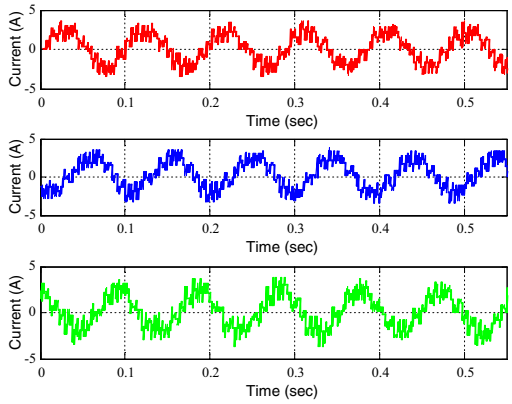

(a) Induction motor phase currents.

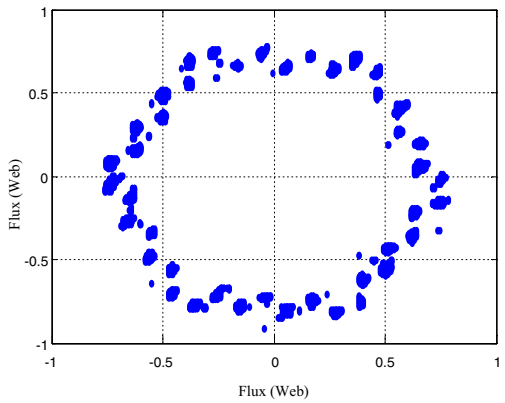

(b) Induction motor stator flux vector trajectory.

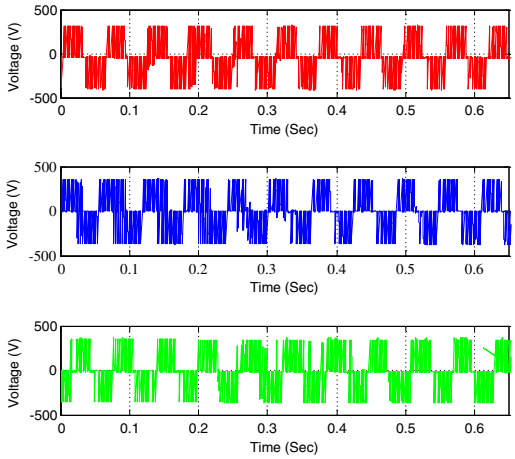

(c) Line-to-line induction motor voltages.

Fig. 16 First induction motor electrical waveforms

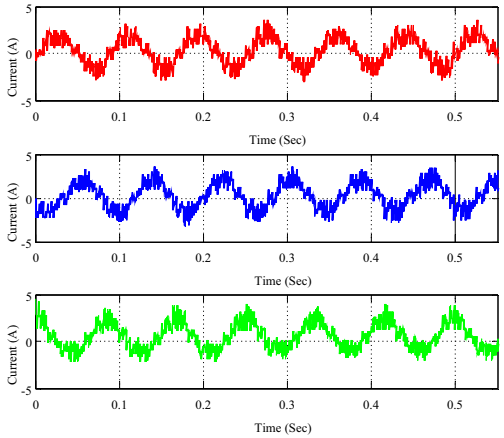

(a) Induction motor phase currents.

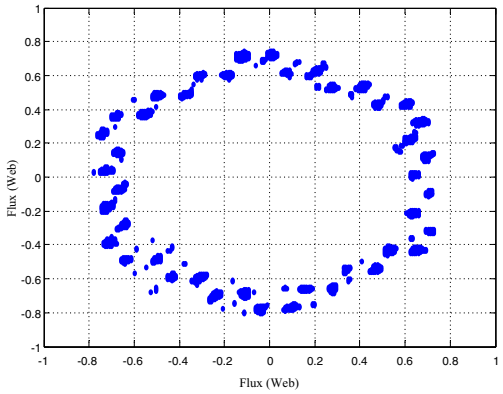

(b) Induction motor stator flux vector trajectory.

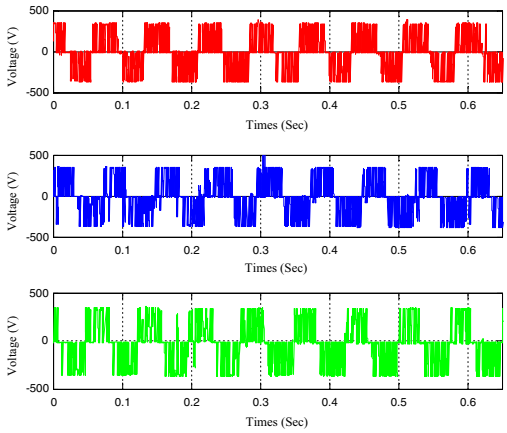

(c) Line-to-line voltages.

Fig. 17 Second induction motor electrical waveforms

6.2 Drive performances with the same torque reference for both motors

At first, both induction motors are operated with the same torque reference.

Figures 16 and 17 present, respectively, the first and second induction motor electromagnetic waveforms. To evaluate the decoupling control, variable speed references are imposed (constant, deceleration, and acceleration).

In Figs. 16a and 17a, we can notice that both motors absorb sinusoidal current leading to few ripples in the motor torque. Figures 16b and 17b represent the stator flux trajectories.

The line-to-line voltages displayed in Figs. 16c and 17c are in accordance with those expected at the output of classical three-phase inverter.

As shown in Fig. 18, there is a good tracking of the speed references for both induction motors.

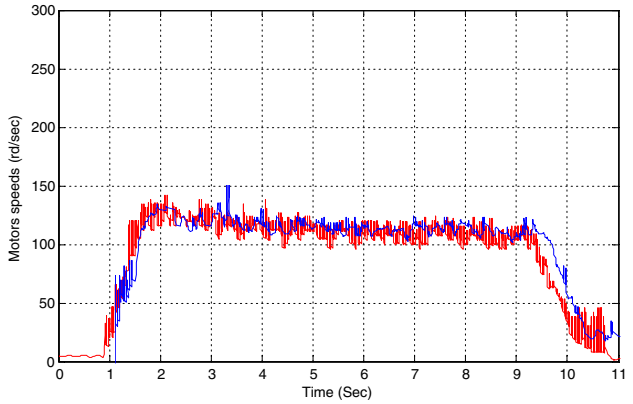

Fig. 18 First and second induction motor speeds (*blue* and *red*, respectively)

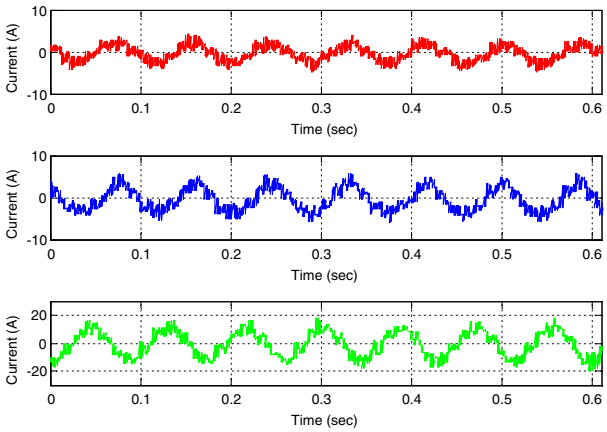

Fig. 19 Common leg current (*green*)—first and second induction motor currents, respectively, (*red* and *blue*)

Figure 19 illustrates the current flowing in the fifth inverter leg (purple line). In this case, the current is sinusoidal with the same frequency as the currents flowing in the other legs but with twice the amplitude.

6.3 Drive performances with different torque references

In the following results, distinct speed references are applied to the induction motors (Figs. 12, 20).

In Fig. 21, the two upper curves represent two currents flowing in each motor and the lower one is the current flowing in the inverter fifth leg.

The above experimental results show that the DTC operates satisfactorily and that the controls of each motor are independent. We can also notice the good behavior of the current flowing in the common leg of the five-leg inverter.

6.4 Electronic differential experimental evaluation

The two following situations have been investigated for the Electronic Differential evaluation:

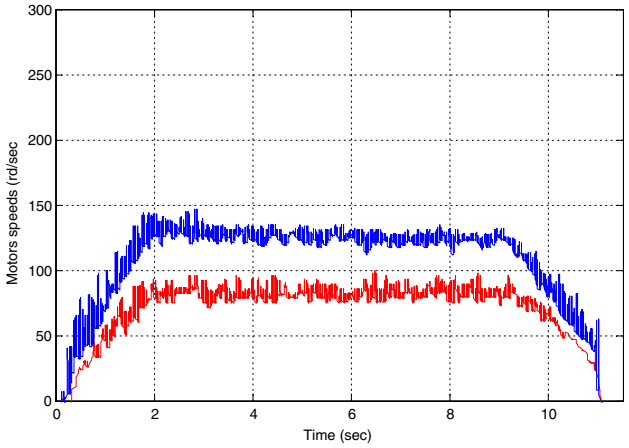

Fig. 20 First and second induction motor speeds (*blue* and *red*, respectively)

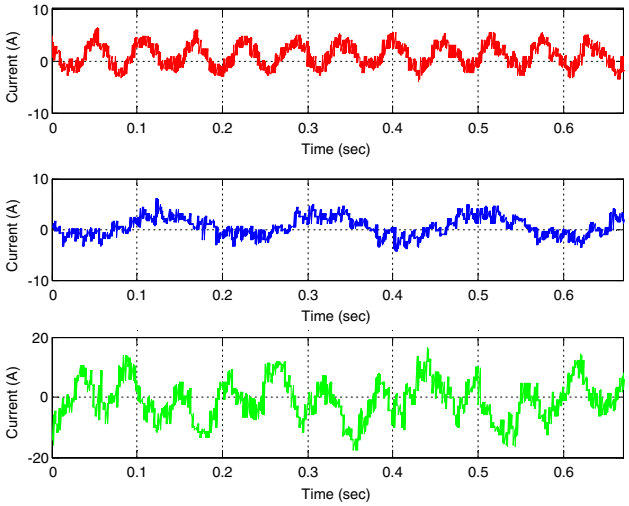

Fig. 21 First and second induction motor currents, respectively, (*red* and *blue*) and common leg current (*green*)

(1) The straightway regime, in which the two motors operate at the same speed and (2) the cornering regime in which each motor runs at a different speed.

Figure 22a illustrates the right (denoted as second) and left (denoted as first) induction motor speeds when the EV is right and left cornering. Three curves are represented: EV trajectory (red), left motor speed (green), and right motor speed (blue). In Fig. 22b, the EV linear speed is given by the red line. In this case, the EV maintains the same speed during different cornering operations.

Figure 22 shows the EV electronic differential responses. The left and right induction motor speeds are displayed when the electric vehicle turns left or right. The results show that the electric differential operates satisfactorily.

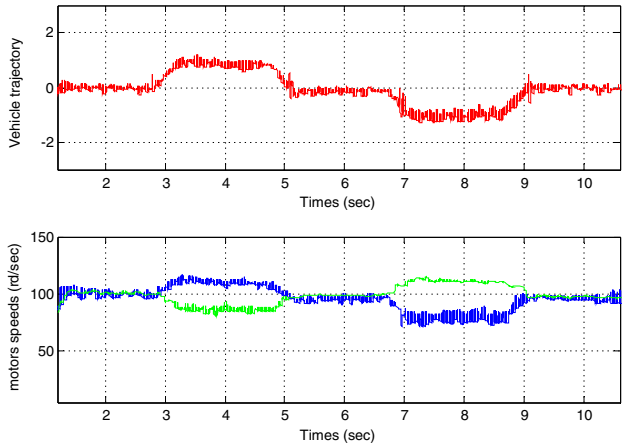

(a) Left and right motor speeds and EV trajectory.

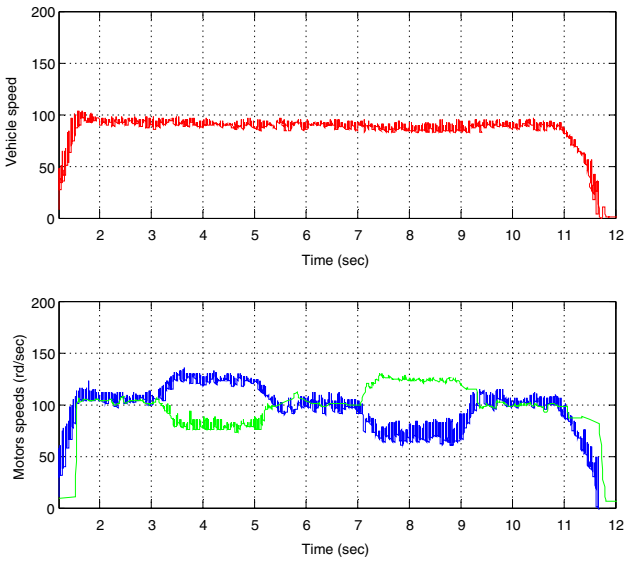

(b) Left and right motorspeeds, and EV linear speed.

Fig. 22 EV electronic differential performances

To validate the proposed independent control with the electric differential, many scenarios are considered with the use of the New European Driving Cycle (NEDC) (Fig. 23) and the Federal Urban Driving Schedule (FUDS) (Fig. 24) [16].

As it can be seen in Fig. 24, for all the speed range, the proposed independent control provides the appropriate speeds to the two wheels to maintain the EV best achievable performances. The simulations results also show the applied electromagnetic torques.

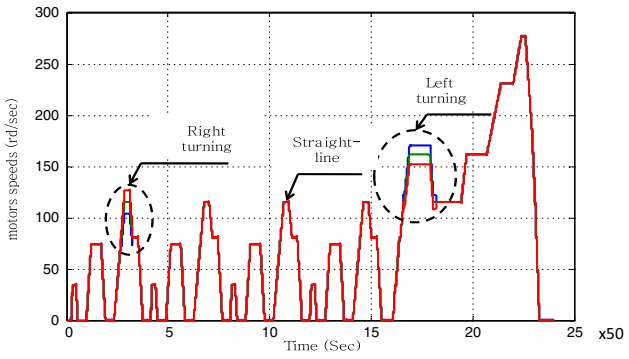

Fig. 23 EV induction motors speeds

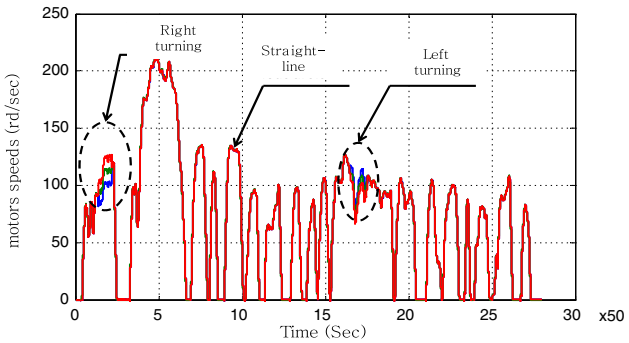

Fig. 24 EV induction motors speeds

7 Conclusion

This paper has described an independent control drive of an electric vehicle. The electric powertrain is built with two induction motors fed with a five-leg inverter, driving the front wheels. Based on direct torque control (DTC) associated with a speed control loop, the independent control is established with a judicious combination of the switching tables initially designed for each motor.

This power conversion structure can be envisaged as a reliable backup solution in case of power-inverter failure in classical powertrains based on three-phase inverters.

The structure also comprises an electronic differential, which by eliminating the mechanical transmission increases the flexibility in the design and reduces the mass and the cost.

After promising simulations results, experimental results with a small-scale test bench (6 kW) have proved the efficacy of the independent control both in terms of speed and torque.

Appendix

EV mechanical and aerodynamic parameters

m = 1540 kg (two 70 kg passengers), A = 1.8 m^2, r = 0.3 m

μ_{rr1} = 0.0055, μ_{rr2} = 0.056, $C_{\text{ad}} = 0.19$, $G = 3.29$, $\eta_g = 0.95$

$v_0 = 4.155$ m/s, $g = 9.81$ m/s^2, $\rho = 0.23$ kg/m^3

Rated data of the simulated induction motor

37 kW, 1480 rpm, $p = 2$

$R_s = 0.0851\,\Omega$, $R_r = 0.0658\,\Omega$

$L_s = 0.0314$ H, $L_r = 0.0291$ H, $L_m = 0.0291$ H,

$J = 0.37$kgm^2, $k_f = 0.02791$N m s

Rated data of the tested induction motor

3 kW, 1420 rpm, p = 2

$R_s = 1.823\Omega$, $R_r = 3.2422\Omega$, $L_s = 0.2289$ H, $L_r = 0.2289$ H, $L_m = 0.2198$ H

$J = 4.1587.10^{-3}$kg m^2, $k_f = 1.277.10^{-3}$N m s/rd

References

1. Jones M, Vukosavic SN, Dujic D, Levi E, Wright P (2008) Five-leg inverter PWM technique for reduced switch count two-motor constant power applications. IET Electric Power Appl 2:275–287
2. Boettcher M, Reese J, Fuchs FW (2013) Reliability comparison of fault-tolerant 3L-NPC based converter topologies for application in wind turbine systems. In: Proceedings of the 2013 IEEE IECON. Vienna, pp 1223–1229
3. Shahbazi M, Poure P, Saadate S, Zolghadri MR (2013) Fault-tolerant five-leg converter topology with FPGA-based reconfigurable control. IEEE Trans Ind Electron 60(6):2284–2294
4. Kimura Y, Hizume M, Matsuse K (2005) Independent vector control of two PM Motors with five-leg inverter by the expanded two-arm modulation method. In: Proceedings of the 2005 EPE. Dresden, pp 1–7
5. Wang W, Cheng M, Zhang B, Zhu Y, Ding S (2014) A fault-tolerant permanent-magnet traction module for subwayapplications. IEEE Trans Power Electron 29(4):1646–1658. http://ieeexplore.ieee.org/xpl/tocresult.jsp?isnumber=6632912
6. Tabbache B, Benbouzid MEH, Kheloui A, Bourgeot JM, Mamoune A (2013) An improved fault-tolerant control scheme for PWM inverter-fed induction motor-based EVs. ISA Trans 52:862–869
7. Dixit A, Mishra N, Sinha SK, Singh P (2012) A review on different PWM techniques for five leg voltage source inverter. In: Proceedings of the 2012 IEEE ICAESM. Tamil Nadu, pp 421–428
8. Lim CS, Rahim NA, Hew WP, Levi E (2013) Model predictive control of a two-motor drive with five-leg-inverter supply. IEEE Trans Ind Electron 60(1):54–65. http://ieeexplore.ieee.org/xpl/tocresult.jsp?isnumber=6296744
9. Khodadoost A, Radan A (2013) Novel comparative study between SVM, DTC and DTC-SVM in five-leg inverter to drive two motors independently. In: Proceedings of the 2013 PEDSTC. Tehran, pp 294–300
10. Haddoun A, Benbouzid MEH, Diallo D (2007) A loss-minimization DTC scheme for EV induction motors. IEEE Trans Veh Technol 56(1):81–88
11. Sutikno T, Idris NRN, Jidin A, Cirstea MN (2012) An improved FPGA implementation of direct torque control for induction machines. IEEE Trans Ind Inf **9**(3):1280–1290. http://ieeexplore.ieee.org/xpl/tocresult.jsp?isnumber=6582568
12. Xia C, Zhao J, Yan Y, Shi T (2014) A novel direct torque control of matrix converter-fed PMSM drives using duty cycle control for torque ripple reduction. IEEE Trans Ind Electron 61(6):2700–2713
13. Patil UV, Suryawanshi HM, Renge MM (2014) Closed-loop hybrid direct torque control for medium voltage induction motor drive for performance improvement. IET Power Electron **7**(1):31–40. http://ieeexplore.ieee.org/xpl/tocresult.jsp?isnumber=6715743
14. El Badsi B, Bouzidi B, Masmoudi A (2013) DTC scheme for a four-switch inverter-fed induction motor emulating the six-switch inverter operation. IEEE Trans Power Electron 28(7):3528–3538
15. Chan CC (2007) The state of the art of electric, hybrid, and fuel cell vehicles. IEEE Proc 95:704–718
16. Tabbache B, Kheloui A, Benbouzid MEH (2010) Design and control of the induction motor propulsion of an electric vehicle. In: Proceedings of the 2010 IEEE VPPC. Lille, pp 1–6 (2010)
17. Chen Y, Wang J (2012) Design and evaluation on electric differentials for overactuated electric ground vehicles with four independent in-wheel motors. IEEE Trans Veh Technol 61(4):1534–1542
18. Haddoun A, Khoucha F, Benbouzid MEH, Diallo D (2007) SDTC neural network traction control of an electric vehicle without differential gears. In: Proceedings of the 2007 IEEE VPPC. Arlington, pp 259–266
19. Perez-Pinal FJ, Cervantes I, Emadi A (2009) Stability of an electric differential for traction applications. IEEE Trans Veh Technol 58(7):3224–3233
20. Tabbache B, Kheloui A, Benbouzid MEH (2011) An adaptive electric differential for electric vehicles motion stabilization. IEEE Trans Veh Technol 60(1):104–110